Laser and Particle Beams

cambridge.org/lpb

Simulations of carbon ion acceleration by 10 PW laser pulses on ELI-NP

D. Sangwan[1], O. Culfa[2,3], C.P. Ridgers[4], S. Aogaki[1], D. Stutman[1,5] and B. Diaconescu[1]

[1]"Horia Hulubei" National Institute for Physics and Nuclear Engineering, Extreme Light Infrastructure – Nuclear Physics ELI-NP, Romania; [2]Department of Physics, University of Nebraska-Lincoln, Lincoln, NE 68588, USA; [3]Department of Physics, Karamanoglu Mehmetbey University, Karaman 70200, Turkey; [4]Department of Physics, York Plasma Institute, The University of York, York YO10 5DD, UK and [5]Department of Physics and Astronomy, The Johns Hopkins University, Baltimore, MD 21218, USA

Research Article

Cite this article: Sangwan D, Culfa O, Ridgers CP, Aogaki S, Stutman D, Diaconescu B (2019). Simulations of carbon ion acceleration by 10 PW laser pulses on ELI-NP. *Laser and Particle Beams* **37**, 346–353. https://doi.org/10.1017/S0263034619000648

Received: 28 May 2019
Accepted: 20 August 2019
First published online: 16 September 2019

Keywords:
Laser–plasma interactions; particle acceleration; PIC simulations

Author for correspondence: O. Culfa, Department of Physics, Karamanoglu Mehmetbey University, Karaman, 70200, Turkey. E-mail: ozgurculfa@kmu.edu.tr

Abstract

We present results of 2D particle-in-cell (PIC) simulations of carbon ion acceleration by 10 petawatt (PW) laser pulses, studying both circular polarized (CP) and linear polarized (LP) pulses. We carry out a thickness scanning of a solid carbon target to investigate the ideal thickness for carbon ion acceleration mechanisms using a 10 PW laser with an irradiance of 5×10^{22} W cm^{-2}. The energy spectra of carbon ions and electrons and their temperature are studied. Additionally, for the carbon ions, their angular divergence is studied. It is shown that the ideal thickness for the carbon acceleration is 120 nm and the cutoff energy for carbon ions is 5 and 3 GeV for CP and LP pulses, respectively. The corresponding carbon ions temperature is ∼1 and ∼0.75 GeV. On the other hand, the energy cutoff for the electrons is ∼500 MeV with LP and ∼400 MeV with CP laser pulses. We report that the breakout afterburner mechanism is most likely causing the acceleration of carbon ions to such high energies for the optimal target thickness.

Introduction

Ion acceleration using multi-petawatt (PW) laser system has been of interest in recent times (Tajima and Dawson, 1979; Esarey *et al.*, 2009; Blaga *et al.*, 2011; Qiao *et al.*, 2012; Bulanov *et al.*, 2014; Gonzalez-Izquierdo *et al.*, 2016; Steinke *et al.*, 2016). One of the main drivers behind these studies is the use of energetic ions for biomedical purposes (Schardt *et al.*, 2010; Ohno, 2013). It includes the potential treatment of tumors by carbon and proton radiotherapy. In laser-based ion acceleration, strong charge-separation electric fields cause the ions to be accelerated to high energies over very short distances. When a PW laser strikes a solid target, copious numbers of hot (>MeV) electrons are launched into the target. As these electrons leave the rear side of the target, a strong charge-separation electric field is set up which scales as $E \sim T_e/\lambda_D$, where T_e and λ_D are the hot electrons temperature and the corresponding Debye length. The field may reach ∼100 TV/m and accelerates ions at the rear surface (Beg *et al.*, 1997; Wilks *et al.*, 2001; Daido *et al.*, 2012; Macchi *et al.*, 2013; Culfa *et al.*, 2014, 2017). This process is called the target normal sheath acceleration (TNSA) (Snavely *et al.*, 2000; Passoni *et al.*, 2010; Macchi *et al.*, 2013).

The laser pulse has momentum which it can deliver to a target. The ion acceleration based on laser beam's pressure is called radiation pressure acceleration (RPA) (Robinson *et al.*, 2008; Henig *et al.*, 2009; Sorbo *et al.*, 2018). The corresponding radiation pressure may go up to $2I/c$. For a 10 PW laser, the radiation pressure is $\sim 3 \times 10^{13}$ atm, where I is the laser intensity and c is the speed of light. In this mechanism, the electrons are pushed inwards in an over-dense target. This motion of electrons leaves a charge separation behind and creates an electrostatic field which in turn acts on the background ions and accelerates them. Further details of ion acceleration by RPA can be found elsewhere (Robinson *et al.*, 2008; Henig *et al.*, 2009; Sorbo *et al.*, 2018; Macchi *et al.*, 2013). In RPA, the ion energy scales with I, whereas in TNSA, it scales with $I^{1/2}$ which shows that RPA acceleration mechanism is favorable at higher intensities.

It is found that ion acceleration beyond the RPA and TNSA energy scaling is possible. The mechanism involved is called breakout afterburner (BOA) (Yin *et al.*, 2007, 2011; Jung *et al.*, 2013). Acceleration by BOA takes place when the target goes transparent after its density has decompressed sufficiently for it to become under-dense. In fact, in the case of PW laser pulses, the density need only decompresses to a_0 times the critical density due to the relativistic mass increase of the electrons. Ion acceleration in the transition to relativistic transparency typically takes place via several phases. Initially, the ion acceleration is due to TNSA as the laser-heated electrons traverse to the rear side. This leads to modest ion energies. This is then followed by the enhanced TNSA phase. In this phase, the laser field heats the background electrons to

CAMBRIDGE UNIVERSITY PRESS

sufficiently high temperature which decreases the plasma frequency ω_p due to the electron's relativistic mass increase. This heating also leads to target expansion and consequent reduction in the electron density, further decreasing ω_p. This leads to the penetration of the laser field in the bulk of the target and initiates the BOA phase. The target electrons are then volumetrically heated, boosting the longitudinal electric field. In the BOA phase, non-linear processes via the growth of electromagnetic instabilities enhance the energy coupling into the ions (Yin *et al.*, 2011). Relativistically induced transparency (RIT) is critical for BOA to occur. RIT is observed when $a_0 \gg \omega_p^2 \ell / 2c\omega_L$, where ω_L is the laser frequency, ℓ is the target thickness, and a_0 is the normalized laser amplitude. Previous experimental studies have shown the acceleration of carbon ions up to 60 MeV per nucleon by this mechanism (Hegelich *et al.*, 2013). Although this represents major progress, it is still less than what is needed for ion beam therapy (~400 MeV/u).

A recent experimental study with laser intensities of $\sim 10^{21}$ W cm^{-2} showed that protons can reach up to ~100 MeV with target thicknesses of ~100 nm (Higginson *et al.*, 2018). It was shown by particle-in-cell (PIC) simulations that protons were accelerated by both RPA and TNSA, which is called hybrid acceleration for linearly polarized (LP) laser pulses (Higginson *et al.*, 2018). Another study with circularly polarized (CP) and LP lasers showed that a CP laser beam is more effective at generating higher energy particles (Zhang *et al.*, 2007). In this paper, a study of C^{+6} ions and electrons acceleration for ultra-thin targets illuminated by ultra-intense (5×10^{22} W cm^{-2}) laser will be presented, considering both LP and CP laser pulses. This is in contrast to recent work investigating ion acceleration with next-generation lasers which has not focused on ion acceleration during the transition to relativistic transparency (Duff *et al.*, 2018; Sorbo *et al.*, 2018). This study has been carried out by 2D PIC simulations. We have investigated the effect of target thickness and laser polarization on particle acceleration and angular divergence of carbon ions.

Simulation setup

We have performed 2D PIC simulations with the relativistic electromagnetic code EPOCH (Ridgers *et al.*, 2014; Arber *et al.*, 2015). As the simulated laser irradiances were well below the threshold for Quantum Electrodynamics (QED) effects (Ridgers *et al.*, 2012), they were not included in our simulations. A thickness scan of solid carbon targets using 2D simulations was carried out. Gaussian CP and LP laser pulses with a peak irradiance of $I = 5 \times 10^{22}$ W cm^{-2} were used in the simulations. The laser pulse struck the target at normal incidence, which was along the x-axis. The beam was focused to a 3 μm focal spot at $y = 0$. We assumed a fully ionized planar target of carbon.

The simulation domain had a size 13 μm × 20 μm and was discretized into 6500 × 2000 cells. This corresponded to a cell size of 2 nm in the x-direction and 10 nm in the y-direction. The box along the x-axis extended between −3 and 10 μm and in the y-axis, between −10 and 10 μm. A total of 300 particles/cell for electrons and 100 particles/cell for C^{6+} were used in the simulations. Open boundary conditions were used for both particles and fields. The laser wavelength (λ) and pulse duration were 0.82 μm and 25 fs, respectively. The corresponding normalized vector potential $a_0 = 8.5 \times 10^{-10} \lambda[\mu\text{m}] \sqrt{I_0[\text{W cm}^{-2}]}$ was ~156. The initial electron density in the target was 6.78×10^{29} m^{-3} which is 400 n_c, where $n_c = 1.1 \times 10^{27} (\lambda[\mu\text{m}])^{-2}$ m^{-3} is the critical electron density. The corresponding initial $\omega_p \sim 5 \times 10^{16}$ rad/s and the skin depth $\ell_p \sim 6 \times 10^{-9}$ m. The carbon target thickness was varied from 10 to 600 nm with a step-like density profile.

We have used short (25 fs) Gaussian laser pulse without prepulse. This was done to make sure that the target of few nm thickness remains intact when the main pulse arrives at the target. As a finite prepulse of high enough magnitude will destroy the nm thick target before the arrival of the main pulse, the study of particle acceleration will be affected (Yin *et al.*, 2011).

PIC simulation results and discussion

Previous work shows that the polarization of the laser pulse affects the particle acceleration (Scullion *et al.*, 2017). Which is confirmed by our simulations. Figure 1 shows the carbon number density for CP and LP laser pulses at different time steps for the target thickness of 120 nm. CP accelerates the ions by RPA, whereas LP causes strong electron heating and so the TNSA mechanism dominates the acceleration of the ions. In LP, carbon acceleration happens in both directions, whereas in CP, carbon is mostly accelerated in the forward direction.

The energy spectra of forward accelerated electron and carbon ions for both CP and LP for different target thicknesses are shown in Figure 2. We can see that maximum kinetic energy (KE) of the accelerated carbon ions is higher in the case of a CP laser (~5 GeV) than for LP (~3 GeV). On the other hand, LP generates higher energy electrons than CP. This difference is thickness-dependent and varies by up to 300%.

Figure 3 shows the mean KE of forward accelerated C^{6+} ions as a function of time for different target thicknesses. From Figure 3, we can see the highest mean KE for both polarizations is obtained when the target thickness is around ~100 nm. This increase in the average KE is more pronounced in case of CP.

This demonstrates the possible role of BOA in ion acceleration in our simulations for both polarizations. In this mechanism, the increase in KE happens when the target becomes transparent to the laser; due to this, the laser pulse penetrates the target and further accelerates the ions via volumetric heating of electrons and generation of electrostatic fields. Transparency occurs due to the decrease in the density and it occurs mainly via three phenomena: (1) the ponderomotive force, which is the force due to laser electric field amplitude gradient, (2) the lowering of the critical density due to the increase in electron mass by fast oscillation in the laser field, and (3) the target expansion due to heating of electrons, which in turn decreases the electron density. All the above-mentioned phenomena collectively reduce ω_p. The sudden increase in ion KE by three to four times is not seen for the thicker targets >200 nm and for much thinner targets <40 nm.

BOA and laser polarization

To understand the effects of both laser polarization and target thickness on particle acceleration, electron and carbon ion energy spectra were examined.

The longitudinal electrostatic field, the laser field, and the density of C^{6+} and electrons for the thickness of 120 nm are shown in Figure 4 at various times. All these quantities are averaged over the size of full width half maximum (FWHM) of the laser pulse. The initial target location is at $x = 0$ μm. Up to 50 fs, we can see that the ion acceleration is due to TNSA, RPA, and the enhanced TNSA. BOA starts between 50 and 75 fs, when the target becomes transparent to the laser. The expansion of the target due to laser ponderomotive pressure and electron heating, in

https://doi.org/10.1017/S0263034619000648 Published online by Cambridge University Press

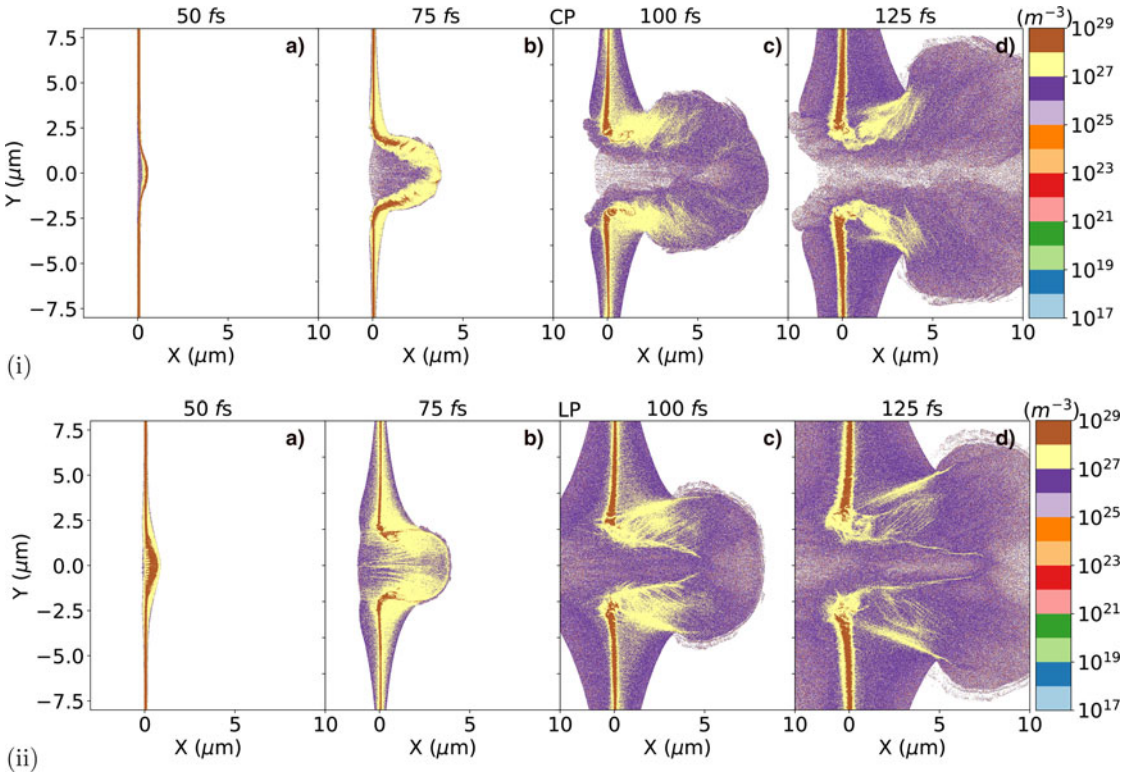

Fig. 1. Time evolution of carbon ion number density (i) for CP laser and (ii) for LP laser pulses, for a 120 nm thick target. A striking difference in acceleration mechanism between LP and CP is noticeable. CP is dominated by the RPA, whereas TNSA dominates in LP.

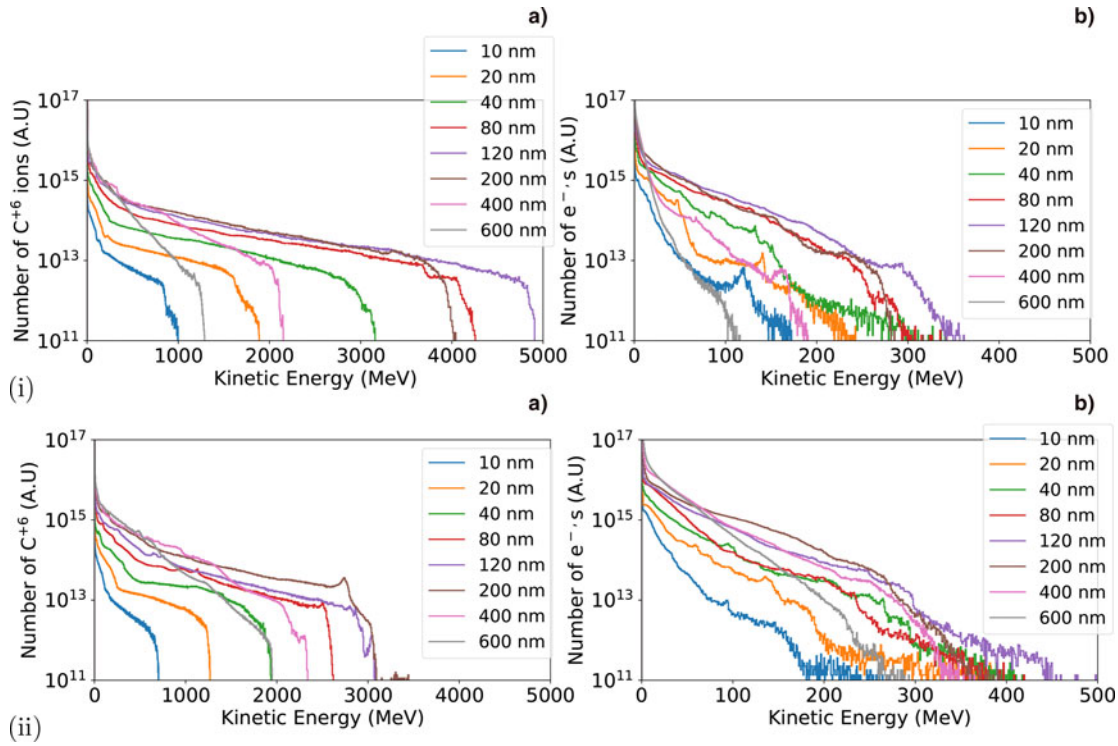

Fig. 2. Energy spectra of carbon ions (left) and electrons (right) for (i) CP and (ii) LP laser beam for different thicknesses.

addition to the relativistic mass increase of the electrons, makes the target transparent. In the transparency phase, the laser penetrates into the target and ions inside the plasma are accelerated by the laser field which leads to an increase in the electric field component in x-direction E_X (see Fig. 4 at 75 fs). It can be seen that BOA has generated a strong longitudinal E_X field and ions are co-traveling with the peak amplitude of the E_X. We can see that during the transparency phase, the electron density is

https://doi.org/10.1017/S0263034619000648 Published online by Cambridge University Press

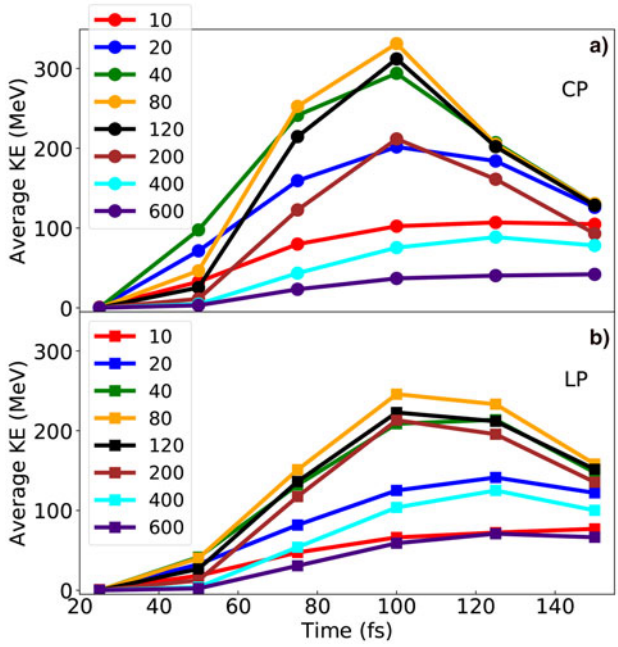

Fig. 3. Average KE of forward accelerated carbon ions, at different time steps for the CP (a) and LP (b) laser beams. Legends show the thickness of the target in nm.

$\sim 2 \times 10^{29}$ m^{-3}, which is $\sim 100 n_c$. As $\gamma \sim 100$, this is the threshold for relativistic transparency. We have seen BOA caused by this transition to transparency for targets of thickness ranging from 40 to 200 nm. However, for thicker targets, it is observed that BOA phase does not occur for CP laser pulses. For these thicknesses, the laser failed to make the target transparent and the acceleration is due to RPA or TNSA.

From Figure 4 (50 fs), we can see that transparency occurs earlier for LP than CP. This leads to a large initial acceleration of carbon atoms in LP but in CP, it takes place at a later stage. The early transparency in LP quickly leads to the BOA phase. Whereas in the CP case, the BOA phase comes later. The required strong E_x field component for the acceleration process lasts up to 100 fs. However, in LP, it lasts for a short duration. The effect of this can be seen from high KE of C^{6+} at 50 fs in LP, but after 50 fs, CP laser acceleration is strong, caused by the large electric field at later times.

Evidence of BOA acceleration has been seen up to the thickness of 200 nm but for larger thickness (400 and 600 nm) transparency and thus BOA do not occur for CP laser pulses (see Fig. 4). However, for the LP case, the target is still transparent so the laser can penetrate through the target and BOA conditions still valid for the thicknesses >200 nm. In CP, the hot electron generation is quenched as compared to LP for these thicknesses. Up to 200 nm, the CP laser pulse generates large cutoff energy C^{6+} ions; however, for the thicker targets, LP laser pulse takes over and causes a sizeable increase in the cutoff energy than the CP laser pulse.

For CP laser pulses and ultra-thin targets with the irradiances $I \sim 10^{21}$ W cm^{-2}, it is observed that the RPA (Esirkepov *et al.*, 2004; Robinson *et al.*, 2008; Tamburini *et al.*, 2010) is the dominant mechanism for the acceleration of protons and heavy ions. For the irradiance studied here ($I = 5 \times 10^{22}$ W cm^{-2}), we see that when the laser is CP, we can still observe the RPA mechanism – except for the optimum target thicknesses where BOA is observed. LP also accelerates ions with RPA and TNSA (hybrid mechanism) mechanism for such high irradiances (Higginson *et al.*, 2018).

The transmission of the laser pulse through the target depends on the pulse duration and intensity along with the thickness of the target. Low-intensity pulses need to have a long pulse duration, on the other hand, high-intensity laser can transmit through the target even at short pulse duration (Petrov *et al.*, 2017). Petrov *et al.* (2017) presented a simple formula from their set of simulations for RPA to RIT transition, $\tau_{\mathrm{FWHM}} \sim 210\sqrt{I[\mathrm{W/cm^2}]/10^{21}}$, where τ_{FWHM} is the required pulse duration for the transparency to occur for a given intensity I. This estimation is for a 20 nm Au

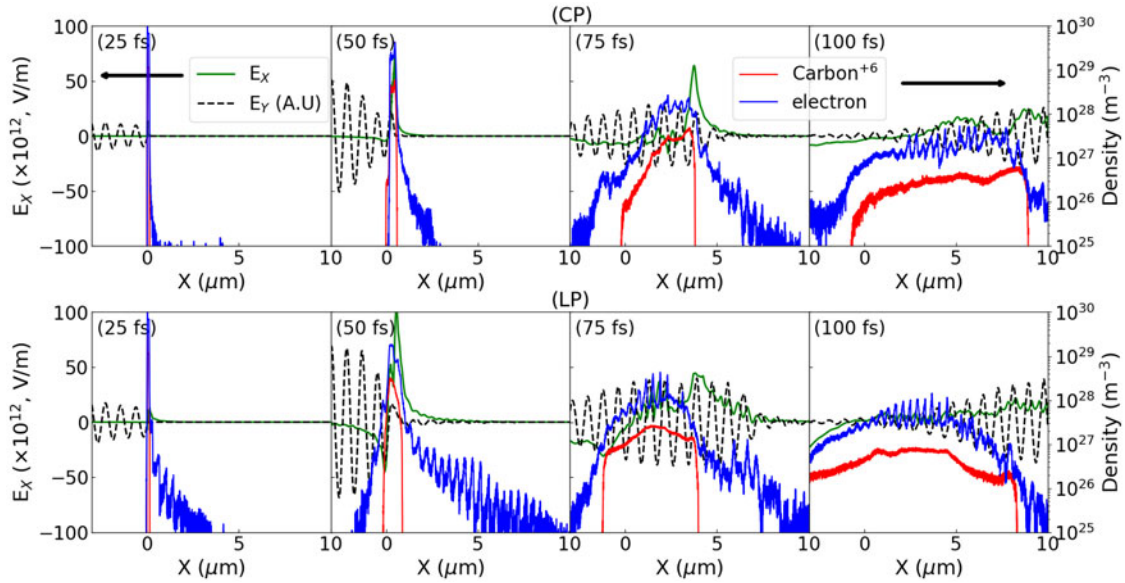

Fig. 4. Time evolution of longitudinal electrostatic electric field E_x, transverse laser field E_y, C^{6+} ions density, and electron density for 120 nm target for both CP (top row) and LP (bottom row). Left scale is for E_x and the right-hand scale represents the carbon and electron density.

https://doi.org/10.1017/S0263034619000648 Published online by Cambridge University Press

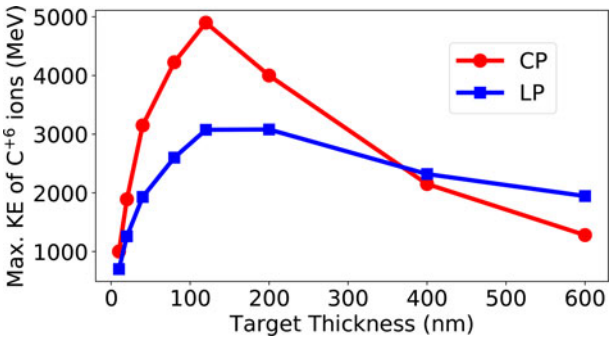

Fig. 5. Maximum energy of carbon ions for LP and CP laser beam at different target thicknesses. The peak KE reaches is observed for the same thicknesses for both polarizations.

target but it can be scaled to align with the thicknesses of the carbon target. Au has electron density $\sim 2500n_c$ and carbon target has $400n_c$, it allows us to take carbon of up to 125 nm. For the former equation given above, by using our PIC simulation parameters, $\tau_{FWHM} \sim 30$ fs can be obtained which is similar to our simulated pulse duration. We have seen RIT occurring up to a 200 nm thick target with a pulse duration of 25 fs, consistent with the formula.

It can be seen that the maximum KE peaks for a 120 nm thick target and then decreases with increasing target thickness (see Fig. 5). In that case, relativistic transparency of the plasma is suppressed and the laser is reflected backward, which causes a drop in the energies of the particles (see Fig. 2). We have shown that laser facilities like ELI-NP (ELI, 2019) are potentially able to accelerate C^{6+} ions up to 5 GeV energies if the laser is CP (see Fig. 5).

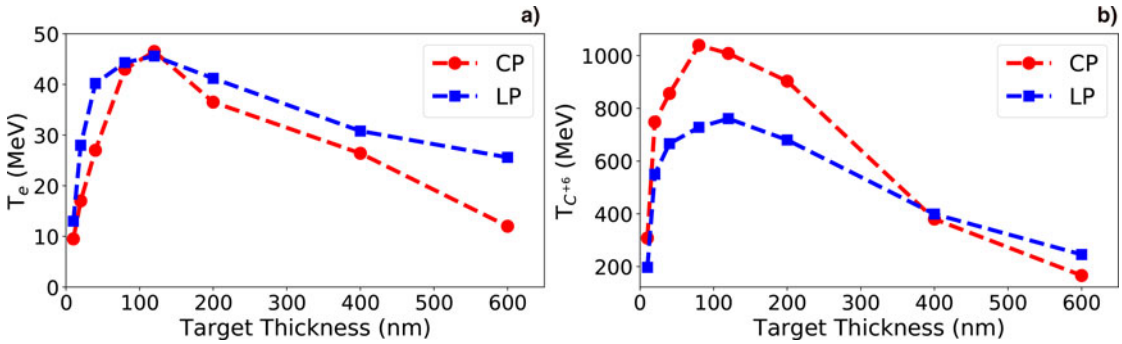

Fig. 6. Comparison of (a) electrons and (b) carbon ions temperatures for LP and CP lasers at different target thicknesses.

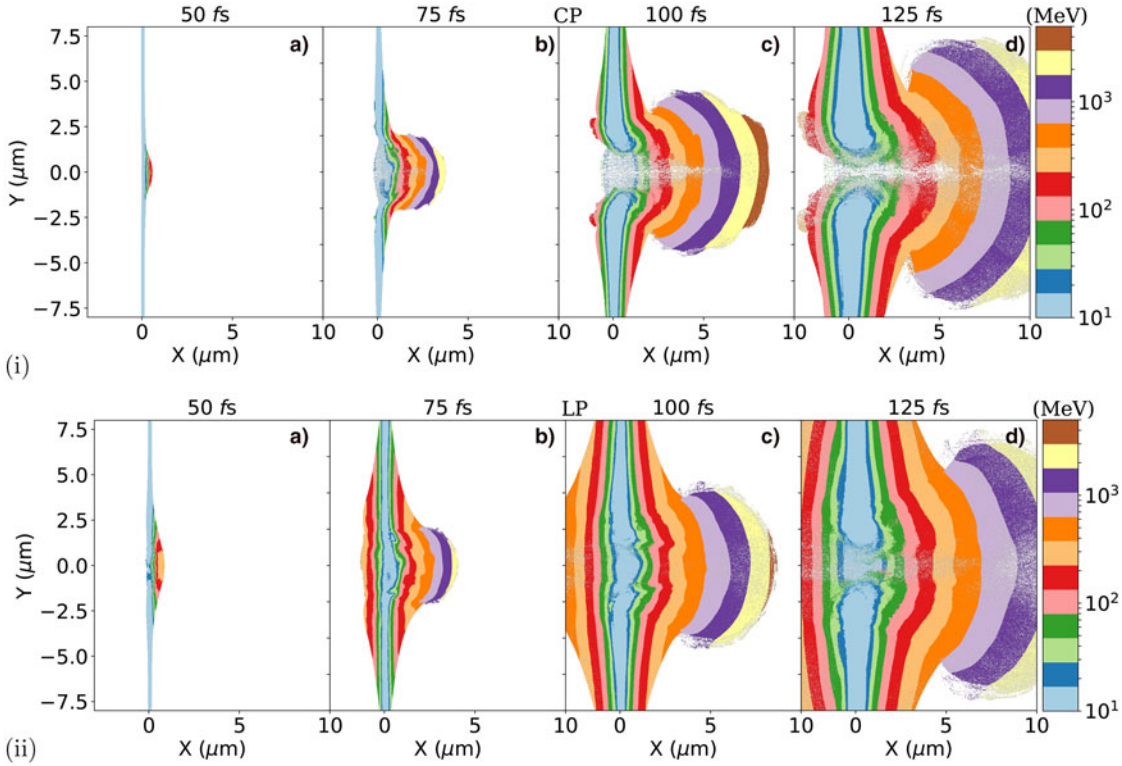

Fig. 7. Time evolution of mean KE of carbon ions for (i) CP, (ii) LP laser beam, for 120 nm target thickness.

https://doi.org/10.1017/S0263034619000648 Published online by Cambridge University Press

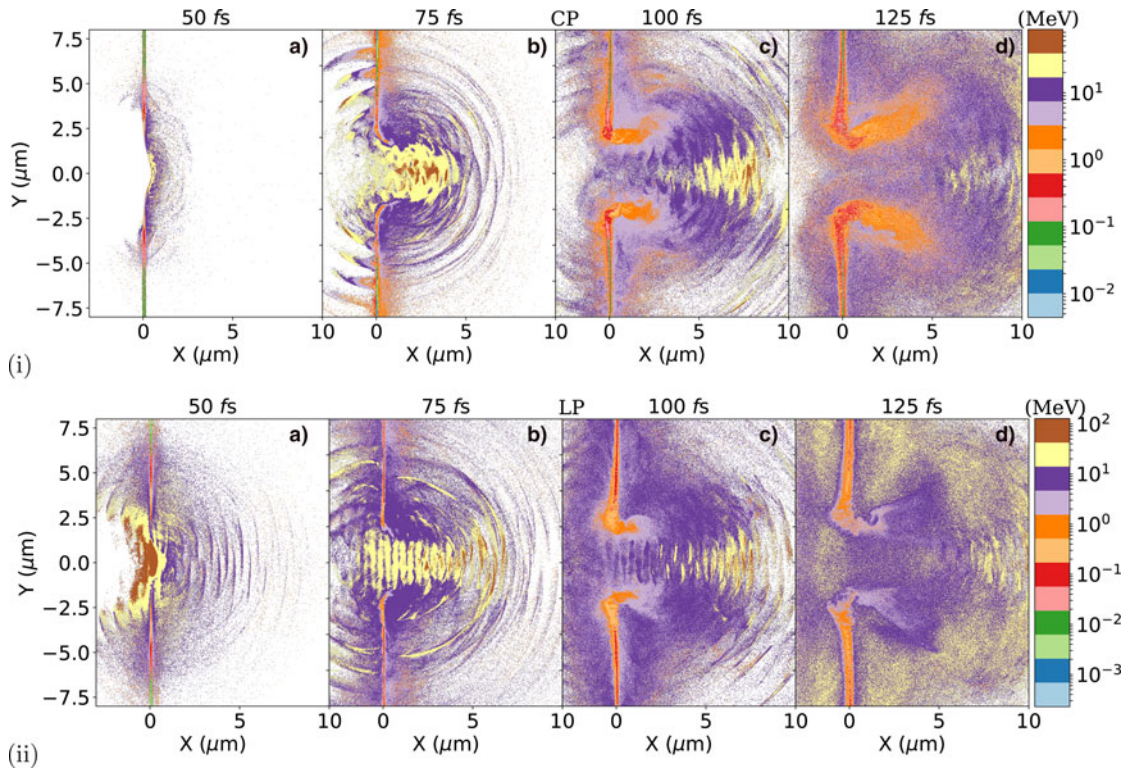

Fig. 8. Mean KE of electrons, at different time steps for (i) CP, (ii) LP laser beam, for 120 nm target thickness.

C^{6+} ions and electrons temperature and mean KE

We have determined the electron and ion temperature (kT) by fitting the electron and ion spectra with exponential of the form exp (−KE/kT). The C^{6+} ion and electron temperature are shown in Figure 6 for the CP and LP laser pulses. For thicknesses of ∼100 nm, the temperature of electrons is ∼40 MeV and for ions, it is ∼1 GeV for a CP laser pulse. In the case of a LP laser pulse, the electrons have the same temperature as the CP laser around the ∼100 nm, but the carbon ion temperature is less than the temperature achieved with CP. The temperature increases until ∼100 nm thicknesses, then it decreases for thicker targets. It suggests that the laser does volumetric heating for targets of up to 200 nm thicknesses. On the other hand, for thicknesses around 400 nm and more, the target becomes impenetrable and volumetric heating does not occur, which brings the temperature down for both species. The C^{6+} ion energies have the same trend as the temperature (see Figs 5 and 6b).

To further analyze the mechanism behind the ion acceleration in CP and LP, we studied the average KE per cell for both C^{6+} ions and electrons. For $\ell = 120$ nm target, Figures 7 and 8 show the mean KE of C^{6+} ions and electrons, respectively. We can see that the radiation pressure of the laser and laser electric field with such irradiances is sufficient to push the electrons and C^{6+} ions through the target for ultra-thin foils. The laser first starts accelerating electrons at the front surface of the target (light pressure) in both polarization cases. CP laser confines and moves together with all charged particles while LP laser first pushes electrons forward sets up a sheath field, and due to charge separation, the ions accelerate both in causing the target to expand (see Figs 7 and 8).

For such thin foils, LP pulses create a hybrid acceleration mechanism which is the combination of RPA and TNSA. Initially, the electrons and C^{6+} ions are accelerated at the front surface of the target (indicating that RPA is the accelerating mechanism), then the TNSA effect on the process shows that ions are accelerated at the back of the target. On the other hand, for the CP laser, acceleration starts at the front surface as well and accelerated charged particles pushed into the target. It shows that in CP laser, acceleration is due to RPA and BOA. The same can be concluded from Figure 8, which shows mean KE per cell of the electrons.

Laser polarization and angular distribution of C^{6+}

The angular distribution of carbon ions is important for future applications. Thus, we have also investigated the C^{6+} ion angular distributions for both CP and LP laser pulses and various thicknesses.

Figure 9 shows the angular distribution of the accelerated carbon ions of KE >500 MeV for different foil thicknesses, for CP and LP laser pulses. We see that laser polarization has no effect on the angular divergence of the C^{6+} ions. It is seen that the angular divergence we report here is in agreement with the previously reported results (Petrov *et al.*, 2017). Regardless of polarization, thicknesses greater than 200 nm are more effective at creating ion beams with small angular distribution as compared to thinner targets. However, increasing target thickness reduces the maximum ion energy and temperature. From Figure 9, we can see that in the case of a CP laser pulse, there are no carbon ions which propagate in the backward direction; however, for an LP laser pulse, a significant number of carbon ions do propagate in the backward direction due to the enhanced electron heating and target expansion for LP.

https://doi.org/10.1017/S0263034619000648 Published online by Cambridge University Press

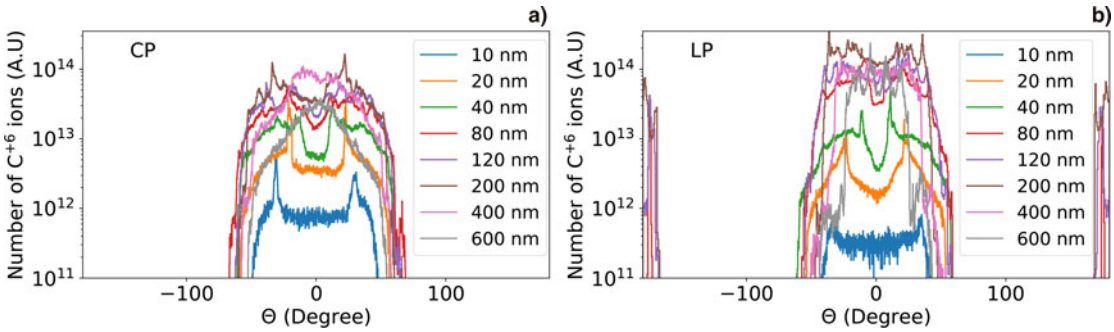

Fig. 9. Carbon ions angular divergence for (a) CP and (b) LP laser beam.

Conclusion

In conclusion, we have investigated the effect of target thickness and laser polarization on particle acceleration and angular divergence in next-generation laser-matter interactions ($I = 5 \times 10^{22}$ W cm^{-2}) by using EPOCH 2D PIC simulations. It is found that the BOA process occurs for targets with thicknesses between 80 and 200 nm, which causes a sudden increase in average ion energy. It is seen that ions can be accelerated ∼5 GeV energies with a target thickness of ∼120 nm by using 10 PW class lasers with CP laser pulses and up to 3 GeV with LP laser pulses. We have shown that the present-day lasers should be capable of generating C^{6+} ions up to 400 Mev/u, which is the required maximum energy for the carbon radiotherapy to treat tumors. We showed that laser acceleration mechanisms have a strong dependence on target thickness as well as laser polarization for 10 PW laser–solid interactions. On simulating different thicknesses, we have found that for the maximum electron and ion energy and temperature, there is an optimum target thickness (∼120 nm) and no dependency on laser polarization for such high irradiances was seen. We have also found that ions are better collimated for target thicknesses of 400 nm or more. We have reported that LP laser turns the target transparent for the thicknesses >200 nm which helps to generate more energetic particles via BOA mechanism, while in CP laser pulse, BOA is not effective for carbon acceleration with those thicknesses (>200 nm). Besides, for CP laser pulses, carbon acceleration takes place in the forward direction only, whereas for LP laser pulses, acceleration in both forward and backward directions occurs.

Acknowledgments. The research was supported by (i) TUBITAK research project 116F042, 118F077 and by Karamanoglu Mehmetbey University Research Project 40-M-16. This work was in part funded by the UK EPSRC grants EP/G054950/1, EP/G056803/1, EP/G055165/1 EP/M018156/1, and EP/ M022463/1, and (ii) the Extreme Light Infrastructure Nuclear Physics (ELI-NP) Phase II, a project co-financed by the Romanian Government and the European Union through the European Regional Development Fund and the Competitiveness Operational Programme (1/07.07.2016, COP,ID 1334).

References

Arber TD, Bennett K, Brady CS, Lawrence-Douglas A, Ramsay MG, Sircombe NJ, Gillies P, Evans RG, Schmitz H, Bell AR and Ridgers CP (2015) Contemporary particle-in-cell approach to laser-plasma modelling. *Plasma Physics and Controlled Fusion* **57**, 113001.

Beg FN, Bell AR, Dangor AE, Danson CN, Fews AP, Glinsky ME, Hammel BA, Lee P, Norreys PA and Tatarakis M (1997) A study of picosecond laser–solid interactions up to 10^{19} W cm^{-2}. *Physics of Plasmas* **4**, 447.

Blaga C, Xu J, DiChiara A, Sistrunk E, Zhang K, Agostini P., Miller T., Mauro LFD and Lin CD (2011) Imaging ultrafast molecular dynamics with laser-induced electron diffraction. *Nature* **483**, 194–197.

Bulanov SV, Wilkens JJ, Esirkepov TZ, Korn G, Kraft G, Kraft SD, Molls M and Khoroshkov VS (2014) Laser ion acceleration for hadron therapy. *Physics Uspekhi* **57**, 1149–1179.

Culfa O, Tallents GJ, Wagenaars E, Ridgers CP, Dance RJ, Rossall AK, Gray RJ, McKenna P, Brown CDR, James SF, Hoarty DJ, Booth N, Robinson APL, Lancaster KL, Pikuz SA, Faenov AY, Kampfer T, Schulze KS, Uschmann I and Woolsey NC (2014) Hot electron production in laser solid interactions with a controlled pre-pulse. *Physics of Plasmas* **21**, 043106.

Culfa O, Tallents GJ, Korkmaz M, Rossall A, Wagenaars E, Ridgers C, Murphy CR, Booth N, Carroll D, Wilson L, Lancaster K and Woolsey N (2017) Plasma scale length effects on protons generated in ultra intense laser plasmas. *Laser and Particle Beams* **35**, 58–63.

Daido H, Nishiuchi M and Pirozhkov A (2012) Review of laser-driven ion sources and their applications. *Reports on Progress in Physics* **75**, 056401.

Duff MJ, Capdessus R, Sorbo DD, Ridgers C, King M and McKenna P (2018) Modelling the effects of the radiation reaction force on the interaction of thin foils with ultra-intense laser fields. *Plasma Physics and Controlled Fusion* **60**, 064006.

ELI (2019) Available at: http://eli-laser.eu.

Esarey E, Schroeder CB and Leemans WP (2009) Physics of laser-driven plasma-based electron accelerators. *Review of Modern Physics* **81**, 1229–1285.

Esirkepov T, Borghesi M, Bulanov S, Mourou G and Tajima T (2004) Highly efficient relativistic-ion generation in the laser-piston regime. *Physical Review Letters* **92**, 175003.

Gonzalez-Izquierdo B, King M, Gray R, Wilson R, Dance R, Powell H, Maclellan D, McCreadie J, Butler N, Hawkes S, Green JS, Murphy C, Stockhausen L, Carroll D, Booth N, Scoot G, Borghesi M, Neely D and McKenna P (2016) Towards optical polarization control of laser-driven proton acceleration in foils undergoing relativistic transparency. *Nature Communications* **7**, 12891.

Hegelich BM, Pomerantz I, Yin L, Wu HC, Jung D, Albright BJ, Gautier DC, Letzring S, Palaniyappan S, Shah R, Allinger K, Horlein R, Schreiber J, Habs D, Blakeney J, Dyer G, Fuller L, Gaul E, Mccary E, Meadows AR, Wang C, Ditmire T and Fernandez JC (2013) Laser-driven ion acceleration from relativistically transparent nanotargets. *New Journal of Physics* **15**, 085015.

Henig A, Kiefer D, Markey K, Gautier DC, Flippo KA, Letzring S, Johnson RP, Shimada T, Yin L, Albright BJ, Bowers KJ, Fernández JC, Rykovanov SG, Wu H-C, Zepf M, Jung D, Liechtenstein VK, Schreiber J, Habs D and Hegelich BM (2009) Enhanced laser-driven ion acceleration in the relativistic transparency regime. *Physical Review Letters* **103**, 045002.

Higginson A, Gray R, King M, Dance R, Williamson S, Butler N, Wilson R, Capdessus R, Armstrong C, Green J, Hawkes S, Martin P, Wei W, Mirfayzi S, Yuan X, Kar S, Borghesi M, Clarke R, Neely D and McKenna P (2018) Near-100 mev protons via a laser-driven transparency-enhanced hybrid acceleration scheme. *Nature Communications* **9**, 724.

https://doi.org/10.1017/S0263034619000648 Published online by Cambridge University Press

Jung D, Yin L, Gautier D, Wu H, Letzring S, Dromey B, Shah R, Palaniyappan S, Shimada T, Johnson R, Schreiber J, Habs D, Fernandez J, Hegelich B and Albright BJ (2013) Laser-driven 1 GeV carbon ions from preheated diamond targets in the break-out afterburner regime. *Physics of Plasmas* **20**, 083103.

Macchi A, Borghesi M and Passoni M (2013) Ion acceleration by superintense laser-plasma interaction. *Reviews of Modern Physics* **85**, 751–793.

Ohno T (2013) Particle radiotherapy with carbon ion beams. *The EPMA Journal* **4**, 9.

Passoni M, Bertagna L and Zan A (2010) Target normal sheath acceleration: theory,comparison with experiments and future perspectives. *New Journal of Physics* **12**, 045012.

Petrov GM, McGuffey C, Thomas AGR, Krushelnick K and Beg FN (2017) Heavy ion acceleration in the radiation pressure acceleration and breakout afterburner regimes. *Plasma Physics and Controlled Fusion* **59**, 075003.

Qiao B, Kar S, Geissler M, Gibbon P, Zepf M and Borghesi M (2012) Dominance of radiation pressure in ion acceleration with linearly polarized pulses at intensities of 10^{21} W cm^{-2}. *Physical Review Letters* **108**, 115002.

Ridgers CP, Brady CS, Ducluos R, Kirk JG, Bennett K, Arber TD, Robinson APL and Bell AR (2012) Dense electron-positron plasmas and ultraintense gamma rays from laser-irradiated solids. *Physical Review Letters* **108**, 165006.

Ridgers C, Kirk J, Duclous R, Blackburn T, Brady C, Bennette K, Arber T and Bell A (2014) Modelling gamma-ray photon emission and pair production in high-intensity laser–matter interactions. *Journal of Computational Physics* **260**, 273–285.

Robinson APL, Zepf M, Kar S, Evans RG and Bellei C (2008) Radiation pressure acceleration of thin foils with circularly polarized laser pulses. *New Journal of Physics* **10**, 013021.

Schardt D, Elsasser T and Schulz-Ertner D (2010) Heavy-ion tumor therapy: physical and radiobiological benefits. *Reviews of Modern Physics* **82**, 383.

Scullion C, Doria D, Romagnani L, Sgattoni A, Naughton K, Symes DR, McKenna P, Macchi A, Zepf M, Kar S and Borghesi M (2017) Polarization dependence of bulk ion acceleration from ultrathin foils irradiated by high-intensity ultrashort laser pulses. *Physical Review Letters* **119**, 054801.

Snavely R, Key M, Hatchett S, Cowan T, Roth M, Phillips T, Stoyer M, Henry E, Sangster T, Singh M, Wilks S, MacKinnon A, Offenberger A, Pennington D, Yasuike K, Langdon A, Lasinski B, Johnson J, Perry M and Campbell E (2000) Intense high-energy proton beams from petawatt-laser irradiation of solids. *Physical Review Letters* **85**, 2945–2948.

Sorbo DD, Blackman DR, Capdessus R, Small K, Slade-Lowther C, Luo W, Duff MJ, Robinson APL, McKenna P, Sheng ZM, Pasley J and Ridgers CP (2018) Efficient ion acceleration and dense electron–positron plasma creation in ultra-high intensity laser-solid interactions. *New Journal of Physics* **20**, 033014.

Steinke S, van Tilborg J, Benedetti C, Geddes CGR, Schroeder CB, Daniels J, Swanson KK, Gonsalves AJ, Nakamura K, Matlis NH, Shaw BH, Esarey E and Leemans WP (2016) Multi stage coupling of independent laser-plasma accelerators. *Nature* **530**, 190–193.

Tajima T and Dawson J (1979) Laser electron accelerator. *Physical Review Letters* **43**, 267–270.

Tamburini M, Pegoraro F, Piazza AD, Keitel CH and Macchi A (2010) Radiation reaction effects on radiation pressure acceleration. *New Journal of Physics* **12**, 123005.

Wilks S, Langdon A, Cowan T, Rooth M, Singh M, Hatchett S, Key M, Pennington D, MacKinnon A and Snavely R (2001) Energetic proton generation in ultra-intense laser–solid interactions. *Physics of Plasmas* **8**, 542.

Yin L, Albright BJ, Hegelich B, Bowers K, Flippo K, Kwan TJT and Fernandez JC (2007) Monoenergetic and gev ion acceleration from the laser breakout afterburner using ultrathin targets. *Physics of Plasmas* **14**, 056706.

Yin L, Albright BJ, Bowers KJ, Jung D, Fernandez JC and Hegelic BM (2011) Three-dimensional dynamics of breakout afterburner ion acceleration using high-contrast short-pulse laser and nanoscale targets. *Physical Review Letters* **107**, 045003.

Zhang X, Shen B, Li X, Jin Z, Wang F and Wen M (2007) Efficient gev ion generation by ultraintense circularly polarized laser pulse. *Physics of Plasmas* **14**, 123108.

https://doi.org/10.1017/S0263034619000648 Published online by Cambridge University Press